Calibrated in-vacuum quantum efficiency system for metallic and III-V thin-film photocathodes

Rasheed, A., Benjamin, C., Elhoussieny, I., Ramachers, Y. and Bell, G.

Rasheed, A., Benjamin, C., Elhoussieny, I., Ramachers, Y. and Bell, G. 2023. Calibrated in-vacuum quantum efficiency system for metallic and III-V thin-film photocathodes. *Journal of Vacuum Science & Technology B.* 41 (6), p. 064006. https://doi.org/10.1116/6.0002904

A calibrated in-vacuum quantum efficiency system for metallic and III-V thin-film photocathodes

Running title: Quantum efficiency for photocathodes

Running Authors: Rasheed et al.

Atif Rasheed[1,3], Christopher Benjamin[2,3], Ibrahim Elhoussieny[3,4], Yorck A. Ramachers[3], and Gavin R. Bell[3a]

1 School of Engineering, Technology and Design, Canterbury Christ Church University, North-Holmes Road, Canterbury, CT1 1QU, UK

2 Vacuum Science Group, STFC Daresbury Laboratory, Keckwick Lane, Daresbury, WA4 4AD, UK

3 Department of Physics, University of Warwick, Coventry, CV4 7AL, UK

4 Department of Physics, Ain Shams University, Cairo, Egypt

[a)] Electronic mail: gavin.bell@warwick.ac.uk

The construction and calibration of a high vacuum system for thin film growth and in situ quantum efficiency (QE) measurement are described. Surface cleaning by in situ argon ion sputtering and annealing is supported. The QE measurement is based on an external 265 nm LED and in situ positively biased collector grid. The system is applied to two metallic and two semiconducting photocathodes: polycrystalline silver and copper, and single crystal InP and InSb. Surface cleaning protocols are shown to have a dramatic effect on the QE for all of these materials. The maximum QE values achieved for clean InSb and InP are around 8×10^{-5}, for Cu 9×10^{-5} and for Ag 2×10^{-4}.

I. INTRODUCTION

Quantum efficiency (QE) is the critical characteristic of a photocathode although other factors such as intrinsic emittance, response time and dark current are also important in different applications.[1] The QE is affected very strongly by surface

condition. Surface oxides and other contamination can suppress photoemission and reduce QE.[2, 3] Conversely, the QE of metallic photocathodes can be enhanced by controlled surface coatings, such as 2D materials on Cu[4] and MgO on Au[5], or by careful surface termination e.g. of Cu-Ba alloys.[6] The sensitivity of QE to surface condition means that a high vacuum (HV) environment is required, and reliable surface preparation protocols are needed. Physical vapor deposition (PVD) is a widely used HV method for thin film growth which can be applied to photocathodes.

The QE system was applied to metal (Ag, Cu) and III-V semiconductor (InSb, InP) samples. Cu and Ag are commonly used metal photocathodes and, as simple metals, are useful for developing understanding of the fundamentals of photoemission. Because of the high QE of Ag, it has found application in photovoltaics[7], glasses[8] and nanocomposites.[9] Cu photocathodes have been widely used in high-luminosity linear colliders and free electron lasers. They are particularly attractive as they allow for the possibility of constructing a simple, all-Cu cavity for the radio frequency gun while providing the robustness necessary for continuous operations over long periods.[10] Qian et al.[11] reported that the performance of Cu photocathodes is significantly influenced by the surface preparation method. With cathode cleaning during rf conditioning, they found that the work function decreased from 4.65 eV to 4.16 eV, and they recorded a QE of 1.5×10^{-4} at $\lambda = 266$ nm, 3.5 times higher than the QE prior to conditioning.

The work functions of single crystal metals vary with crystal face, with Ag between 4.10 eV and 4.53 eV, and Cu between 4.56 eV and 4.90 eV. Typically, Ag has a correspondingly higher QE than Cu. Nonetheless, it is not just the work function which defines the QE at a given excitation wavelength. The surface reconstruction and localised

surface electronic states can be very important. For example, Cu (001) should have higher QE than Cu(111) as the former has lower work function. However, Cu(111) has higher QE than Cu(001) because of the presence of favorable surface states. Similarly, for 2D materials on metal photocathodes, it has been suggested that the effective doping of graphene on polycrystalline Cu is affected by alterations in local work function through crystallographic changes induced by annealing [12]. The computed QE for polycrystalline Cu and Ag are 1.1×10^{-4} and 1.9×10^{-4}, respectively [13], while a very broad range of QE has been reported in the literature for Ag and Cu $(10^{-6} - 10^{-3})$. The latter suggests that the surface condition (contamination, oxides) can overwhelm the effects of surface crystalline structure.

InP and InSb are direct gap semiconductors with room temperature band gaps 1.34 eV and 0.17 eV respectively. Both InP and InSb can produce large current densities up to the limit of the Child-Langmuir law suggesting that these materials can be used to develop intense electron sources.[14] In this study of InP(111) and InSb(111), QE values in the range 10^{-4} – 10^{-5} at λ = 222 nm were reported.[14]

In this work, we have developed a HV system which combines PVD growth, surface cleaning and in situ QE measurement at fixed wavelength of 265 nm. The system is described and its application to metallic and semiconductor photocathodes is outlined. The importance of surface cleaning for both III-V semiconductor photocathodes (InSb and InP) and metallic photocathodes (Cu, Ag) is highlighted. The highest QE values achieved for clean InSb and InP are around 8×10^{-5}, while clean Cu reached 9×10^{-5} and Ag 2×10^{-4}.

II. EXPERIMENTAL

A. System design

The HV system is shown in Fig. 1 with key components labelled. It is based

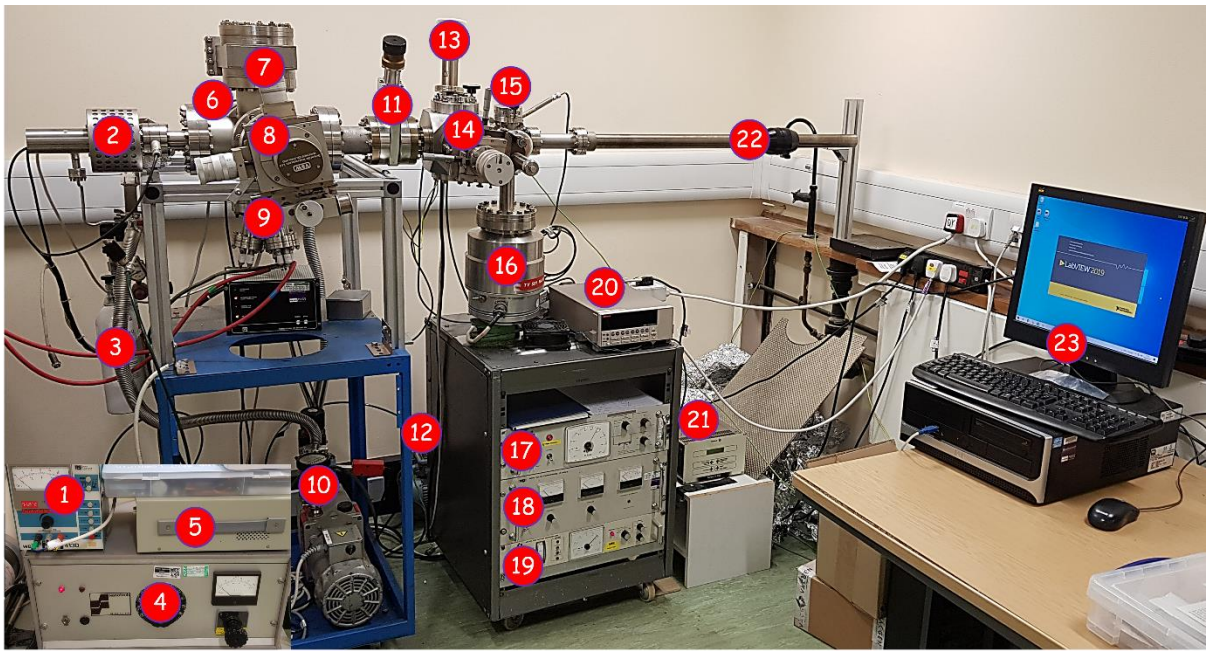

1. *Power supply for sputter gun*
2. *Magnet and sputter gun*
3. *Argon gas bottle*
4. *Power supply for metallic source*
5. *Power supply for sample heating*
6. *Turbo pump for treatment chamber*
7. *Sample treatment chamber*
8. *Sample holder with attached thermocouple*
9. *Metallic sources with shutters*
10. *Rotary pump for treatment chamber*
11. *Mechanical valve to transfer samples between treatment and quantum efficiency chambers*
12. *Rotary pump for quantum efficiency chamber*
13. *Ultraviolet torch with wavelength of 265 nm*
14. *Quantum efficiency chamber*
15. *Load lock*
16. *Turbo pump for quantum efficiency chamber*
17. *Control unit for Pirani gauge in quantum efficiency chamber*
18. *Control unit for sputter gun*
19. *Control unit for Pirani gauge in treatment chamber*
20. *Keithley 6485 pico-ammeter*
21. *Control unit for turbo pump in quantum efficiency chamber*
22. *Transfer arm*
23. *LabView program to plot data from Keithley 6485 pico-ammeter through RS-232 port*

FIG. 1. Two-chamber HV system for PVD and in situ QE measurement.

around two stainless steel six-way cross ConFlat chambers (7 and 14) connected by a valved tube. A magnetic linear transfer arm allows samples to be moved between the chambers, and also loaded from ambient air into the smaller chamber (15). “Flag”-style sample plates are used, giving a maximum sample size of approximately 12 mm × 12 mm. The smaller chamber acts as both the load-lock and the QE measurement chamber, while the larger chamber allows PVD and surface cleaning by argon ion sputtering (2).

The sample plate sits on an x-y-z-θ manipulator in the PVD chamber which is equipped with a Ta heater filament and thermocouple to allow controlled sample annealing to 600°C. A cluster flange (9) incorporates two home-built effusion cells for PVD growth of Mg and Ag respectively. The cells can be shuttered from the sample by a Ta shield mounted on a rotary feedthrough on the third port of the cluster flange. Pure oxygen can be introduced into the PVD chamber using an all-metal leak valve, and argon can be introduced through the same gas manifold for sputtering. The gas manifold can be pumped independently to a pressure of 10^{-2} mbar. Both chambers are turbomolecular pumped, and the PVD chamber can reach pressures in the 10^{-9} mbar range. The pressure during QE measurements is typically in the low 10^{-8} mbar range.

The QE measurement is shown in Fig. 2. The sample faces upwards in an earthed

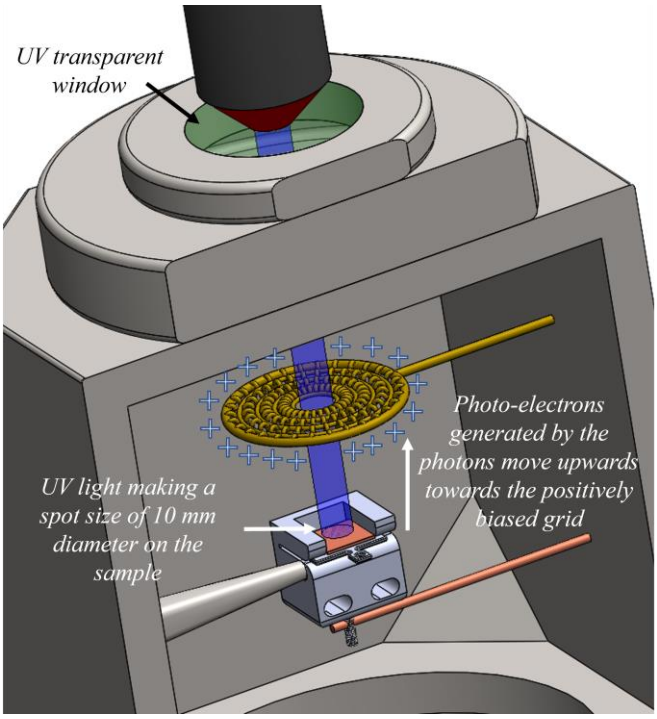

FIG. 2. Schematic of the QE arrangement.

holder, which is mounted on a small x-y-z-θ stage to allow loading from the main transfer arm. It is moved to the measurement position below (1) a circular electrode of 40 mm diameter with a central hole, and (2) a fused silica ConFlat window with 98% transmission down to around 230 nm. Mounted above the window (in air) is a 265 nm UV LED with focusing lens. This produces a 10 mm diameter spot on the sample (spot size and position are checked periodically with a UV phosphor card). The transmitted power was measured directly to be 0.10 mW using a calibrated photodiode, allowing the photocurrent measured on the collection electrode to be converted into an absolute QE. The collection electrode is positively biased using a series of three 9V batteries to ensure that all photocurrent was collected (additional bias voltage produces no additional current). The photocurrent was measured using a pico-ammeter, whose output was collected via RS232 interface on a computer as a time series. The measured photocurrent typically settles to a steady value within a few tens of seconds, with some temporal differences observed depending on whether pico-ammeter is turned on before or after the UV LED. The time dependence may be associated with capacitances in the circuit, for example around the vacuum feedthrough. A separate test of a similar feedthrough alone in a simple battery – resistor circuit indeed produced a few seconds of "settling time" in the current. The electrode is a fixed 60 mm distance away from the sample. During development of the system, the geometry, bias voltages and LED power were varied and no evidence for space-charge effects was observed.

The photocurrent noise is low (electrical screening and good earthing from the stainless steel HV chamber, short external cable length) and QE values in the 10^{-8} to 10^{-4} range can be measured. The random error in QE measurements is better than 1%. To convert

photocurrent to QE, an absolute calibration of incident optical power is needed. This was achieved by replicating the geometrical setup, including the fused silica window, on the benchtop. A silicon photodiode sensitive down to at least 200 nm wavelength (Thorlabs S120VC) was positioned at the equivalent sample position (± 1 mm). The aperture of the photodiode is 9.8 mm meaning 96% of incident light is captured at the specified distance. Power measurements were taken from a Thorlabs PM400 optical power meter. The specification for the photodiode states a resolution of 1 nW, power range of 50 nW – 50 mW and an uncertainty of ± 7 % for the wavelengths 200 – 279 nm. The effects of the distance error are slightly enhanced by the photodiode aperture size and were estimated geometrically, but are significantly smaller than the photodiode's measurement uncertainty. Combining these errors in the incident power calibration, we can assign a systematic uncertainty of 8% to the QE derived from the photocurrent.

The PVD growth chamber allows two elements to be deposited either individually or in tandem. Vapor pressures can be controlled in the range 10^{-8} to 10^{-7} mbar giving a wide range of growth rates depending on the application. The cold cathode argon ion source is typically operated with ion energies in the range 2 – 3 keV giving a sample current of several μA. There is no in situ chemical or structural analysis available such as X-ray photoemission spectroscopy or electron diffraction, and so growth "recipes" must be adapted from other PVD systems or refined using ex situ thin film analysis. The system has been used so far to grow ultra-thin MgO on Ag samples and to deposit Ag films on Cu and other substrates. In this paper we discuss only argon ion sputter / anneal results.

B. Materials

Ag and Cu foil samples were as-rolled, ~ 0.15 mm thick, $\geq 99.98\%$ purity, supplied by ANALAR, DBH Laboratory Chemicals Ltd. (UK). Single crystal InP(001) and InSb(001) samples were supplied by Wafer Technology Ltd. (UK). The samples were polished and epi-ready. The InP is n-type, $(1-10) \times 10^{18}\ cm^{-3}$, while the InSb is low-doped p-type, $\sim 5 \times 10^{15} cm^{-3}$. However, the argon ion sputter and anneal treatment may induce additional n-type doping near the sample surfaces. Foil samples were easily cut to size with scissors, while the III-V wafers could be cleaved to size, with any dust from the cleave blown off using N_2.

C. Sample production

Four batches of samples were prepared. The first batch was initially cleaned by mechanical abrasion using silicon carbide (SiC) and then chemical-mechanical polishing using a household metal polish. Following this chemical-mechanical cleaning, samples were ultrasonically cleaned in acetone then isopropyl alcohol for ten minutes each. These samples are labelled MCU-AR ("mechanical, chemical, ultrasonicate – as-received"). The second batch, coded MCUAO-AR (added "acetic-ozone"), was further cleaned by dipping into acetic acid and then cleaned for 30 min. using a UV ozone cleaner (Ossila Ltd, UK). As well as measuring QE as-received, both batches were also degassed at 300 ℃ for 1 hour, argon-ion sputtered for 30 min., followed by annealing at 300 ℃ for a further hour. These are named MCU-SA and MCUAO-SA, respectively ("sputter-anneal").

III. RESULTS AND DISCUSSION

Typical QE time series scans are shown in Fig. 3 for (a) Ag, (b) Cu, (c) InP and (d) InSb. The low noise and good convergence to a steady value are clear. Different colours represent the four protocols of cleaning. All four samples recorded increases in QE after the additional acetic acid dip and ozone cleaning (black to blue) although this improvement was marginal for InP [the black data in panel (c) level off at almost the same value as the blue]. The QE further increased with sputtering and annealing (black to green, blue to red). The increase of QE from sputtering and annealing is quite consistent for all four materials after both MCU and MCUAO treatments. The highest QE is reached after the most comprehensive cleaning protocol, MCUAO-SA. The final QE

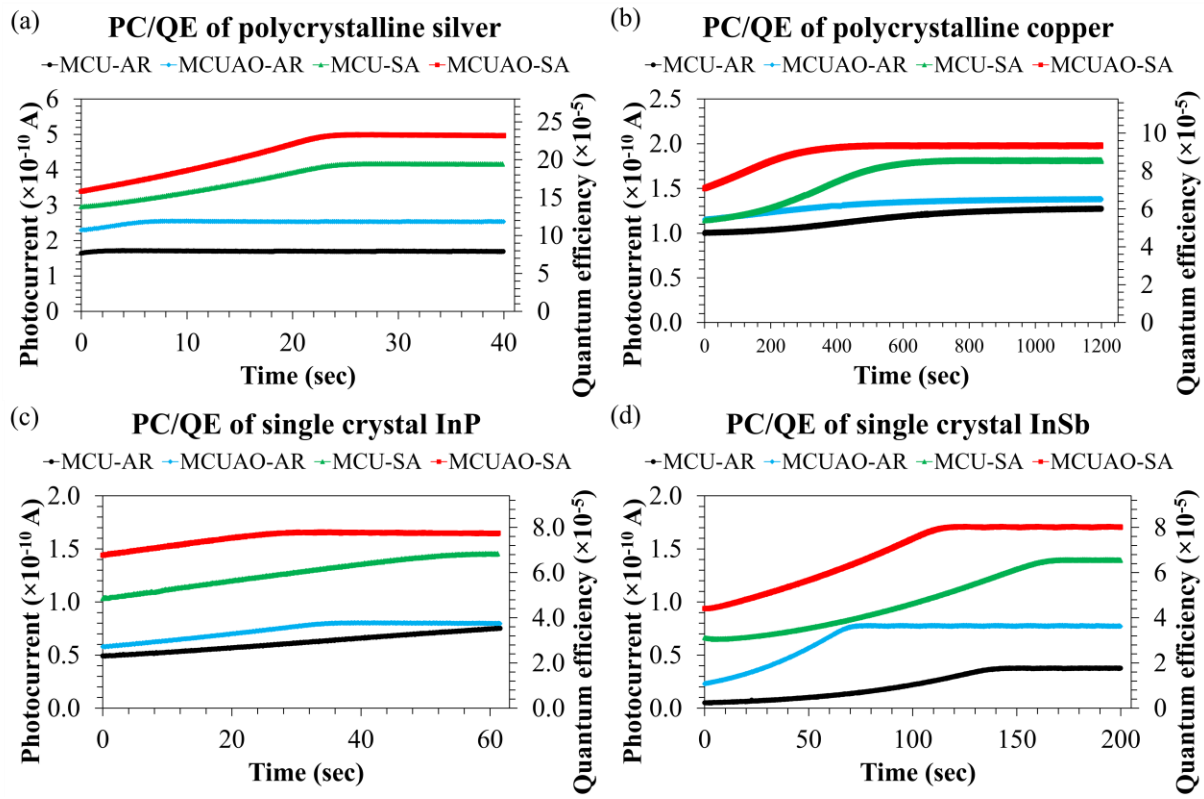

FIG. 3. Photocurrent and quantum efficiency values of (a) polycrystalline silver, (b) polycrystalline copper, (c) single crystal InP, and (d) single crystal InSb.

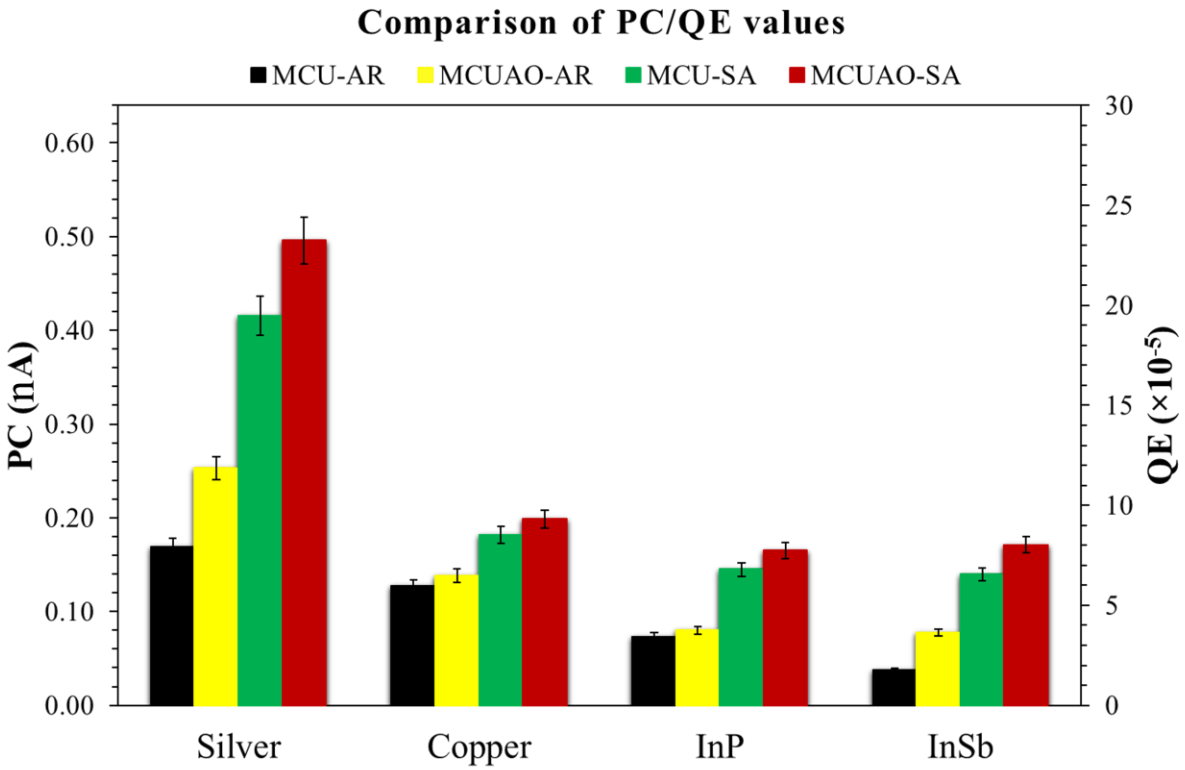

FIG. 4. Comparison of photocurrent and quantum efficiency values for the four materials as a function of surface cleaning protocol.

values are plotted in Fig. 4. The highest QE was 2.32×10^{-4} for Ag MCUAO-SA samples.

Anjum et al.[15] used magnetron sputtering to deposit polycrystalline Ag on a quartz substrate. They measured QE after transfer through air and without local surface cleaning. With a 250 nm UV LED, they recorded QE $(8.77 \pm 0.90) \times 10^{-6}$ and $(1.20 \pm 0.12) \times 10^{-6}$ in reflection and transmission modes, respectively. Anjum et al. were able to expose their Ag photocathodes to air for 72 hours without further degradation of the QE. However, the reflection QE value is much lower than found in this work, presumably due to surface contamination during air transfer. As electrons have very short inelastic scattering length in metals (~ 1 nm), the photoelectric effect becomes

very sensitive to surface contamination.[16] Around half of the photoelectrons are generated from the topmost atomic plane and only $\sim 11\%$ from the second atomic layer, for Ag and Cu.[13] Hence, even a few monolayers of contamination, generated in a few seconds of air exposure, could seriously reduce the QE. Henneken et al.[17] found an increase in QE by a factor 3 for Cu(111) after argon ion sputtering and annealing. Our increases are smaller, but this may reflect the improved surface condition after the chemical-mechanical-ozone cleaning steps.

The overall behaviors of InP and InSb were rather similar after ion sputtering despite the large difference in fundamental band gap. This suggests that the surface Fermi level may well be stabilized near the conduction band minimum and that energy level relative to the vacuum level is principally derived from the indium electronic states. Our QE values are consistent with those reported by Arneodo et al.[14] for slightly shorter wavelength light.

IV. SUMMARY AND CONCLUSIONS

We have discussed the design and build of a vacuum system for combined PVD thin film growth and QE measurements. The QE measurements use an external 265 nm LED with focusing optics, a positively biased collector electrode and a standard pico-ammeter. The PVD chamber hosts two shuttered effusion cells, presently Mg and Ag. The system includes an argon ion gun for sputter cleaning and samples can be annealed in HV. This in situ cleaning is shown to improve the QE of both metal and semiconductor photocathodes even after careful ex situ cleaning via chemical and mechanical means. The absolute QE values for the cleanest InSb and InP photocathode surfaces are around 8×10^{-5}, for Cu 9×10^{-5} and for Ag 2×10^{-4}. The system will allow rapid and flexible

prototyping of photocathode thin films with fast, accurate monitoring of QE. Future developments will include swappable external LED housings to allow QE at multiple wavelengths to be measured. Extension of the chamber for compatibility with a vacuum suitcase is also planned.

ACKNOWLEDGMENTS

The work was supported by STFC (UK) via project number ST/V002325/1, and through a Warwick Collaborative Postgraduate Research Studentship held jointly with the STFC Accelerator Science and Technology laboratory. Ibrahim G. Elhoussieny thanks the Egyptian Higher Education Ministry for funding his PhD (Ref: MM5/18). We are grateful to Lee Jones and Tim Noakes for valuable discussions.

DATA AVAILABILITY

Data available on request from the authors.

AUTHOR DECLARATIONS

A. Conflict of interest

The authors have no conflicts to disclose

REFERENCES

1. A. Aspect, P. Grangier, and G. Roger, *Phys. Rev. Lett.* 47, 460 (1981).
2. I. Schnitzer, E. Yablonovitch, C. Caneau, and T. J. Gmitter, *Appl. Phys. lett.* 62, 131 (1993).
3. A. Breskin, *Nucl. Instruments Methods Phys. Res. Sect. A Accel. Spectrometers, Detect. Assoc. Equip.* 371, 116 (1996).

4. G. Wang, P. Yang, N. A. Moody, and E. R. Batista, *npj 2D Mater. Appl.* 2 (2018).

5. I. A. Napier, V. Chang, T. C. Q. Noakes, and N. M. Harrison, *Phys. Rev. Appl.* 11, 064061 (2019).

6. D. Motta and S. Schönert, *Nucl. Instruments Methods Phys. Res. Sect. A Accel. Spectrometers, Detect. Assoc. Equip.* 539, 217 (2005).

7. Y. Shi, X. Wang, W. Liu, T. Yang, R. Xu, and F. Yang, *J. Appl. Phys.* 113, 176101 (2013).

8. C. Strohhöfer and A. Polman, *Appl. Phys. Lett.* 81, 1414 (2002).

9. C. Flytzanis, F. Hache, M. C. Klein, D. Ricard, P. Roussignol, and E. Wolf, *Ed. by E. Wolf, Elsevier Sci. Publ. BV* (1991).

10. K. Batchelor, R. C. Fernow, J. Fischer, A. S. Fisher, J. Gallardo, G. Ingold, H. G. Kirk, K. P. Leung, R. Malone, J. Rogers, T. Tsang, J. Sheehan, S. Ulc, M. Woodle, J. Xie, R. S. Zhang, L. Y. Lin, C. M. Hung, and X. J. Wang, *Nucl. Instruments Methods Phys. Res.* A318, 372 (1992).

11. H. J. Qian, C. Li, Y. C. Du, L. X. Yan, J. F. Hua, W. H. Huang, and C. X. Tang, *Phys. Rev. Spec. Top. - Accel. Beams* 15, 040102 (2012).

12. F. Le Pimpec, C. J. Milne, C. P. Hauri, and F. Ardana-Lamas, *Appl. Phys. A Mater. Sci. Process.* 112, 647 (2013).

13. B. Camino, T. C. Q. Noakes, M. Surman, E. A. Seddon, and N. M. Harrison, *Comput. Mater. Sci.* 122, 331 (2016).

14. F. Arneodo, F. Cavanna, I. De Mitri, D. Mazza, and V. Nassisi, *Rev. Sci. Instrum.* 72, 63 (2001).

15. F. Anjum, H. Nasir, J. Lee, and H. J. Kim, *Opt. - Int. J. Light Electron Opt.* 269, 169906 (2022).

16. H. Ebel, M. Mantler, R. Svagera, and R. Kaitna, *Surf. Interface Anal.* 22, 602 (1994).

17. H. Henneken, F. Scholze, and M. Krumrey, *Metrologia* 37, 485 (2000).